Journal of Fluids and Structures (2001) **15,** 981–1007
doi:10.1006/jfls.2001.0387, available online at http://www.idealibrary.com on IDEAL®

NUMERICAL INVESTIGATION OF A ROTATIONALLY OSCILLATING CYLINDER IN MEAN FLOW

M. CHENG

Institute of High Performance Computing
89B Science Park Drive #01-05/08, The Rutherford Singapore Science Park I
Singapore 118261, Singapore

AND

Y. T. CHEW AND S. C. LUO

Department of Mechanical Engineering, National University of Singapore
Singapore 117576, Singapore

(Received 10 November 2000, and in final form 10 April 2001)

Vortex shedding and the development of a wake behind a rotationally oscillating circular cylinder was investigated using a hybrid vortex method at a Reynolds number of 1000 over a wide range of forcing frequency and amplitude. The normalised peripheral velocity–oscillation amplitude of the cylinder ranged from 0 to 3 while the ratio of forcing frequency to the vortex-shedding frequency from a stationary cylinder varied from 0 to 10. The time-dependent pressure, lift and drag forces exerted on the cylinder were studied together with the flow patterns in the wake. Some behaviours of vortex shedding are revealed and the lock-on range for vortex shedding is obtained. It is found that, in the case of a very low frequency ratio, vortices are shed at a frequency close to that from a stationary cylinder when the amplitude is small; however, the vortices are shed at cylinder-oscillation frequency when the amplitude is large. When the frequency ratio is close to 1, the form of vortex shedding and lock-on exhibit a particularly strong resonance between the flow perturbations and the vortex wake, and the mean value of the drag coefficients increases remarkably. Its maximum value increases with increasing amplitude within the lock-on range and shifts towards the lower frequency end of the lock-on range. When the frequency ratio is greater than a certain value beyond the lock-on range, small-scale vortices are shed at the forcing frequency in the near wake. Subsequently, these vortices coalesce and result in a large-scale antisymmetrical structure in the far wake similar to the Kármán vortex street past a stationary cylinder. The mean value of the drag coefficients decreases in the post lock-on frequency range. The larger the amplitude, the more distinct is the drag coefficient decrease, and the minimum value is lower than that for flow past a stationary cylinder. After the minimum is reached, the drag coefficient increases again with further increase in cylinder-oscillation frequency and approaches the value for the stationary cylinder.

1. INTRODUCTION

THE STUDY OF VORTEX SHEDDING from an oscillating bluff body has fascinated researchers for a long time. The occurrence of this flow phenomenon is due to instabilities and depends on the geometry of bluff body and the Reynolds number. It has often been the cause of flow-induced failure of structures in various fields of engineering. The study of periodic vortex shedding and wake development behind a bluff body remains to be one of the most challenging problems in fluid mechanics, since it can lead to better understanding of the cause of vortex-induced vibration and its subsequent suppression and control.

0889–9746/01/070981 + 27 $35.00/0

Studies on flow past an oscillating cylinder can be divided into the following two categories depending on the motion of the cylinder. In the first category, the cylinder oscillates translationally at an angle of 0° or 90° with respect to the free stream. They are in-line and transverse oscillation, respectively. Many experimentalists (Bishop & Hassan 1964; Koopmann 1967; Taneda 1972; Griffin & Ramberg 1974; Bearman & Currie 1979; Bearman 1984; Ongoren & Rockwell 1988a, b; Williamson & Roshko 1988) had shown that the vortex shedding phenomenon can be dramatically altered for the cylinder undergoing in-line and transverse oscillation in a fluid stream. For in-line oscillations, vortex lock-on occurs when the oscillation frequencies are approximately twice the Strouhal frequency (the frequency of the vortex shedding from a stationary cylinder). For transverse oscillations, lock-on usually occurs near the Strouhal frequency (Griffin & Hall 1991; Meneghini & Bearman 1995).

In the second category, the cylinder performs a rotational oscillation about its axis in mean flow. It is well known that lock-on or resonance occurs when the body and wake oscillations have the same frequency that is near one of the characteristic frequencies of the structures. Vortex lock-on can also be realised with rotational oscillations of a circular cylinder. However, in contrast to the fairly large number of studies conducted in the first category, there is relatively little research carried out in this category.

Viscous flow around a rotationally oscillating cylinder was investigated experimentally by Okajima *et al.* (1975) for Reynolds numbers (Re) of 40–160 and 3050–6100. Their results showed that, when the oscillation frequency of the cylinder is at or near the frequency of vortex shedding from a stationary cylinder, the vortex shedding synchronises with the cylinder motion. Taneda (1978) studied the effects of rotational oscillation at $\mathrm{Re} = 30$–300, and showed that, at very high oscillation frequencies, the stagnant-fluid region behind the cylinder, as well as the vortex-shedding process, could be nearly eliminated. Wu *et al.* (1989) and Wu (1990) carried out work similar to Okajima *et al.* (1975), at $\mathrm{Re} = 300$ and 500. Their results showed that, when the forcing frequency is equal to that of the natural vortex-shedding frequency of the cylinder, the shed vortices in the wake become more organised, and both the unsteady lift and drag components reach their maximum. Wu also suggested that the drag could decrease below that of a stationary cylinder when the frequencies are mismatched.

More recently, the frequency response of the shear layers separating from a circular cylinder undergoing small amplitude rotational oscillation has been investigated experimentally by Filler *et al.* (1991) in water at a Reynolds number range of 250–1200. By referencing the lock-on analyser to the cylinder oscillations, the amplitude and phase of the response to different frequency oscillations were measured directly. They found that rotational oscillations corresponding to cylinder peripheral speeds of between 0.5 and 3% of the free-stream velocity can be used to influence the primary (Kármán) mode of vortex generation. For Re greater than 500, such oscillations can also excite the shear-layer vortices associated with the instability of separating shear layers. Exploratory experiments have also been carried out by Tokumaru & Dimotakis (1991) on circular cylinders executing forced rotational oscillations in a steady uniform flow. They examined the efficacy of rotational oscillation as an actuation mechanism for active control of the cylinder wake. Their experiments showed that working in a control domain, in which the structures of vortices shed are synchronous with the forcing frequency, provides the greatest control authority over the wake structure and the flow phenomena observed are qualitatively the same over a large range of Reynolds numbers. Their results also showed that rotational oscillation at very large magnitudes can produce significant reduction in the drag acting on the cylinder when the forcing frequency and the stationary cylinder vortex-shedding frequency are mismatched.

The effects of rotationally oscillating cylinder on vortex shedding and wake are of considerable practical interest from the standpoint of wake modification and the reduction of flow-induced vibration. In particular, it is of interest to determine whether at a given Reynolds number, there is a lock-on range that is similar to the cases of a circular cylinder undergoing in-line and transverse oscillations in a free stream. On the other hand, although certain aspects of the behaviour of flow past a rotationally oscillating cylinder had been investigated by some researchers (Wu *et al.* 1989; Tokumaru & Dimotakis 1991; Filler *et al.* 1991) by using some visualisation techniques, due to the limitations of the experimental equipment, it is difficult to capture the detailed processes of the fluid–body and vortex–vortex interactions. The above can be overcome by certain numerical simulation techniques.

The earlier numerical studies concerning vortex shedding from a rotationally oscillating cylinder in a uniform flow were carried out by Lu & Sato (1996) at Re = 200, 1000 and 3000. The primitive variable form of the Navier–Stokes equations for incompressible flows was solved numerically by a fractional step method. The interest of their investigations is flow structures of vortex formation and the numerical studies are mostly limited to the cases of frequency ratio f_c/f_0 of 0·5, 1, 2, 3 and 4, and the normalised peripheral velocity amplitude in the range 0·1 to 3. According to their computed results, the large-scale vortex structures in the near wake are nearly the same for Re = 200, 1000 and 3000. In the range of their calculated parameters, the lift coefficients vary at the same vortex-shedding frequencies for $f_c/f_0 \leq 3$. However, for higher oscillating frequencies, the frequency of the lift variation is less than that of the vortex shedding for $f_c/f_0 = 4$. Similar work was carried out by Chou (1997). Recently, using a spectral-finite difference method, the flow induced by a rotationally oscillating and translating circular cylinder was investigated by Dennis *et al.* (2000) at Re = 500 in a range of $f_c/f_0 = 0{\cdot}883$–$2{\cdot}5$, and Re = 1000 at two values of $f_c/f_0 = 1{\cdot}25$ and 2·5. The normalised oscillating amplitude is fixed at 1. They found that, for $f_c/f_0 = 2{\cdot}5$, the near wake does not involve adjacent corotating vortex coalescence, and as a result of this, the usual behaviour of the drag coefficient is observed. This is rather unlike the case when Re = 500. Thus, the Reynolds number seems to have more influence on the structures and the fluid forces at higher forcing frequency than at lower values, which is in contrast with the finding of Lu & Sato (1996). However, the common points of interest of the investigations are flow structures of vortex formation at different Reynolds number, and the numerical studies are mostly limited to the cases of vortex-shedding resonance. At low Reynolds number, the quasiperiodicity in the wake of a rotationally oscillating cylinder is studied by Baek & Sung (2000). A direct numerical simulation is made to portray the unsteady dynamics of wake flows at Re = 110. The normalised forcing frequency f_c/f_0 varies in a range of 0·87–1·1 and the velocity amplitude of oscillation is 5% of the free-stream velocity. They found that, within the lock-on regime, the shedding frequency bifurcates with one frequency following the forcing frequency while the other gradually converges to the natural shedding frequency.

In the present work, the unsteady flow past a rotationally oscillating circular cylinder is studied numerically over a much wider range of forcing frequency and amplitude. A hybrid vortex method, which was previously presented and applied to the situation of flow past a rotating circular cylinder (Chew *et al.* 1995; Cheng *et al.* 1997), is used to simulate this type of flow at the same Reynolds number, Re = 1000. This Reynolds number is identical to that investigated by Lu & Sato (1996) and Dennis *et al.* (2000) for two-dimensional flow. Although it is well known that three-dimensional effects begin to occur when Re > 180 for flow past a stationary circular cylinder, it is not unreasonable to believe that the transitional Reynolds number would be much higher for a rotationally oscillating cylinder since a strong two-dimensional rotational disturbance is imposed on the flow. As the present

method is very efficient computationally, it allows computation over a long period in order to investigate the development of vortex wake and the global behaviour of lift and drag force. The approach used to understand the vortex-formation process is to trace the motion of fluid particles, which leads to streaklines similar to those observed in a smoke wire flow visualisation. The primary objective is to investigate the influence of the oscillating amplitude and forcing frequency in both lock-on and nonlock-on regimes on the wake structure, pressure distributions, lift and drag force on the cylinder. The secondary objective is to determine the basic vortex-shedding structure in the near wake, the lock-on regime, and the parameter range in which the mean value of drag force is lower than that for flow past a stationary cylinder.

2. GOVERNING EQUATIONS AND NUMERICAL METHOD

Consider the two-dimensional flow of a viscous incompressible fluid of constant velocity $\tilde{U}_\infty$ past a rotationally oscillating cylinder of radius $\tilde{a}$. The cylinder rotates sinusoidally at an angular velocity $\tilde{\omega}(\tilde{t})$, which gives

$$\tilde{U}_w(\tilde{t}) = \tilde{a}\tilde{\omega}(t) = \tilde{A}_m \sin(2\pi \tilde{f}_c \tilde{t}), \tag{1}$$

where $\tilde{U}_w$ is the peripheral velocity of the cylinder, $\tilde{A}_m (= \tilde{a}\tilde{\omega}_{\max})$ is the velocity amplitude of the cylinder oscillation, $\tilde{\omega}_{\max}$ is the maximum value of the angular velocity, and $\tilde{f}_c$ is the oscillating frequency. The origin of the frame of reference $(\tilde{r}, \theta)$ coincides with the centre of the cylinder which oscillates rotationally about its own axis.

The governing equations in dimensionless form for the flow are

$$\frac{\partial \zeta}{\partial t} - \mathrm{e}^{-2\xi} \frac{\partial(\psi, \zeta)}{\partial(\xi, \theta)} = \frac{2}{\mathrm{Re}} \mathrm{e}^{-2\xi} \left(\frac{\partial^2 \zeta}{\partial \xi^2} + \frac{\partial^2 \zeta}{\partial \theta^2} \right), \tag{2}$$

and

$$\frac{\partial^2 \psi}{\partial \xi^2} + \frac{\partial^2 \psi}{\partial \theta^2} = -\mathrm{e}^{2\xi} \zeta. \tag{3}$$

The relationship of between stream function (ψ) and vorticity (ζ) with velocity ($\mathbf{u}$) is described by

$$\mathbf{u} = \nabla \times (\psi \mathbf{k}), \quad \zeta \mathbf{k} = \nabla \times \mathbf{u}. \tag{4}$$

The boundary conditions for $t \geq 0$ defined by the problem of equations (2) and (3) are

$$\psi = 0, \quad \frac{\partial \psi}{\partial \xi} = -A_m \sin(2\pi f_c t) \quad \text{at } \xi = 0, \tag{5}$$

$$\mathrm{e}^{-\xi} \frac{\partial \psi}{\partial \xi} \to \sin\theta, \quad \zeta = 0 \quad \text{as } \xi \to \infty, \tag{6}$$

$$\psi(\xi, \theta, t) = \psi(\xi, \theta + 2\pi, t), \quad \zeta(\xi, \theta, t) = \zeta(\xi, \theta + 2\pi, t) \tag{7}$$

and the vorticity boundary condition on the surface of the cylinder is determined from the Poisson equation (3) (Cheng *et al.* 1997).

The following dimensionless variables are introduced:

$$r = \frac{\tilde{r}}{\tilde{a}}, \quad \mathbf{u} = \frac{\tilde{\mathbf{u}}}{\tilde{U}_\infty}, \quad \psi = \frac{\tilde{\psi}}{\tilde{U}_\infty \tilde{a}}, \quad \zeta = \frac{\tilde{a}\tilde{\zeta}}{\tilde{U}_\infty}, \quad t = \frac{\tilde{U}_\infty \tilde{t}}{\tilde{a}},$$

$$f = \frac{\tilde{a}\tilde{f}}{\tilde{U}_\infty}, \quad A_m = \frac{\tilde{a}\tilde{\omega}_{\max}}{\tilde{U}_\infty}, \quad \mathrm{Re} = \frac{2\tilde{a}\tilde{U}_\infty}{\tilde{\nu}}, \tag{8}$$

where the tilde denotes the dimensional variables, $\tilde{r}$ and θ are the usual cylindrical polar co-ordinates, $\xi = \ln r$, $\tilde{t}$ is the time, $\tilde{\nu}$ is the kinematic viscosity, and $\tilde{f}$ represents either the vortex-shedding frequency ($\tilde{f}_v$) or the cylinder-oscillating frequency ($\tilde{f}_c$).

The lift, drag, pressure and shear-stress coefficients are defined according to

$$C_L = \frac{\tilde{F}_L}{\tilde{\rho}\tilde{U}_\infty^2 \tilde{a}}, \quad C_D = \frac{\tilde{F}_D}{\tilde{\rho}\tilde{U}_\infty^2 \tilde{a}}, \quad C_p = \frac{\tilde{p} - \tilde{p}_\infty}{\frac{1}{2}\tilde{\rho}\tilde{U}_\infty^2}, \quad C_\sigma = \frac{\tilde{\sigma}_{r\theta}}{\frac{1}{2}\tilde{\rho}\tilde{U}_\infty^2}, \tag{9}$$

where $\tilde{F}_L$, $\tilde{F}_D$, $\tilde{p}$ and $\tilde{\sigma}_{r\theta}$ are lift, drag, pressure and shear stress exerted by the fluid on a unit length of the cylinder, respectively, $\tilde{p}_\infty$ is the static pressure at infinity, and $\tilde{\rho}$ is the fluid density.

The pressure and shear-stress distributions on the surface of the cylinder are obtained from the following integration:

$$C_p = 1 - U_w^2 + 2\int_1^\infty \left(\frac{2}{\mathrm{Re}}\frac{1}{r}\frac{\partial \zeta}{\partial \theta} + \frac{\partial u_r}{\partial t} - u_\theta \zeta\right) \mathrm{d}r, \tag{10}$$

$$C_\sigma = \frac{4}{\mathrm{Re}}\left[r\frac{\partial}{\partial r}\left(\frac{u_\theta}{r}\right)\right]_{r=1}. \tag{11}$$

The pressure and the shear-stress components of the drag and lift coefficients are obtained from the following integrations:

$$C_{Dp} = -\frac{1}{2}\int_0^{2\pi} C_p \cos\theta \, \mathrm{d}\theta, \quad C_{Lp} = -\frac{1}{2}\int_0^{2\pi} C_p \sin\theta \, \mathrm{d}\theta, \tag{12}$$

$$C_{D\sigma} = -\frac{1}{2}\int_0^{2\pi} C_\sigma \sin\theta \, \mathrm{d}\theta, \quad C_{L\sigma} = -\frac{1}{2}\int_0^{2\pi} C_\sigma \cos\theta \, \mathrm{d}\theta. \tag{13}$$

The total drag and lift coefficients are given by

$$C_D = C_{Dp} + C_{D\sigma}, \quad C_L = C_{Lp} + C_{L\sigma}. \tag{14}$$

A hybrid vortex method is used to solve the above problem. It is based on a combination of diffusion-vortex method and vortex-in-cell method by dividing the flow field into two regions. In the region near the body surface the diffusion-vortex method is used to solve the governing equations, while the vortex-in-cell method is used in the exterior domain. The accuracy and applicability of the method have been described and lot of tests have been conducted to determine the optimum mesh size and time step by the authors in detail in two previous papers (Chew *et al.* 1995; Cheng *et al.* 1997). Here, the region near the body surface corresponds to $0 \le \xi \le 0{\cdot}4$ and the exterior domain corresponds to $0{\cdot}4 < \xi \le \xi_\infty$. An optimal grid system of $I \times J = 257 \times 513$ nodes is chosen (Cheng *et al.* 1997), where I and

J are the number of grid points in the ξ and θ direction, respectively. The calculation for the present problem starts at $t_0 = 0{\cdot}001$, using the Rayleigh solution for the value of vorticity. The optimal nondimensional time step chosen is $\Delta t = 0{\cdot}02$.

In this paper, the velocity amplitude A_m of the cylinder oscillation ranges from 0 to 3 while the frequency ratio f_c/f_0 varies from 0 to 10. Many cases were investigated within these ranges. However, for brevity, only selected cases will be presented. The special case of flow past a stationary circular cylinder ($f_c/f_0 = 0$) has been investigated in earlier work (Chew *et al.* 1995). When Re = 1000, $\bar{C}_D = 1{\cdot}14$, the frequency f_0 is equal to 0·103 and the Strouhal number ($2f_0$) is equal to 0·206.

3. SMALL VELOCITY AMPLITUDE OSCILLATION WITH $A_m = 0{\cdot}25$ AND Re = 1000

3.1. Pattern of Vortex Shedding from the Cylinder in the Near Wake

The near-wake vortex-shedding patterns represented by the streaklines are shown in Figure 1 for the small velocity amplitude oscillation with $A_m = 0{\cdot}25$.

When $f_c/f_0 = 0{\cdot}2$, it is seen from Figure 1(a) that alternately shed vortices which have approximately the same strength advance downstream and the vortex-shedding frequency f_v is equal to f_0. As the shed vortices shed move steadily away from the cylinder in the downstream direction, the streaklines exhibit periodic fluctuation with the same frequency as vortex shedding, as if the behaviour of vortex shedding in the near wake is not affected by the oscillation of the cylinder. In actual fact, when the frequency of the cylinder oscillation is very low, the effect of the oscillation can gradually appear in the far wake as time increases. This will be observed from the time history of lift coefficient later.

In the range $0{\cdot}4 \leq f_c/f_0 \leq 0{\cdot}6$, although vortices are still shed alternatively at a frequency f_v that is close to the frequency f_0, the strength and size of vortices shed become different. One interesting phenomenon that is observed is that a weaker and smaller vortex is shed once every two or three cycles as shown in Figure 1(b). This is more clearly demonstrated in the animated flow visualisation when the variation with time is captured continuously. This phenomenon can be explained in terms of the interaction between the oscillating cylinder and the fluid. In the range $0{\cdot}4 \leq f_c/f_0 \leq 0{\cdot}6$, the vortex strength is weaker when the rotational oscillation decreases the relative velocity between the fluid and the side of the cylinder where the vortex is to be shed, mainly because of the decreased generation of vorticity in the boundary layer. Within this range of f_c/f_0 where f_c is not synchronised with f_0, such an event occurs once in every two to three cycles of vortex shedding.

When $f_c/f_0 = 0{\cdot}8$, the patterns of streaklines evolution are found to be basically the same as those at $f_c/f_0 = 0{\cdot}2$. Vortices similar in size but with opposite sign are shed from both sides of the cylinder as shown in Figure 1(c). However, the vortex-shedding frequency f_v is no longer equal to f_0. In fact, vortices are shed at the frequency f_c. This means that the cylinder and the vortex shedding have the same characteristic frequency ($f_v = f_c$) and lock-on or resonance has taken place. When f_c/f_0 increases to 1·2, the phenomena that one out of every two or three vortices shed by the cylinder is weaker in strength and smaller in size is observed again, as shown in Figure 1(d). The asymmetric pattern of vortex shedding is broken down.

As f_c/f_0 further increases, the process of vortex formation is completely different from that of the previous cases. Figure 1(e) shows that, at $f_c/f_0 = 5$, the small-scale vortices of opposite sign are generated at the frequency f_c from both sides of the cylinder, and they "assemble" behind the cylinder and form a large-scale vortex which is then detached from the cylinder. In other words, the vortex does not detach from the cylinder until both its strength and size

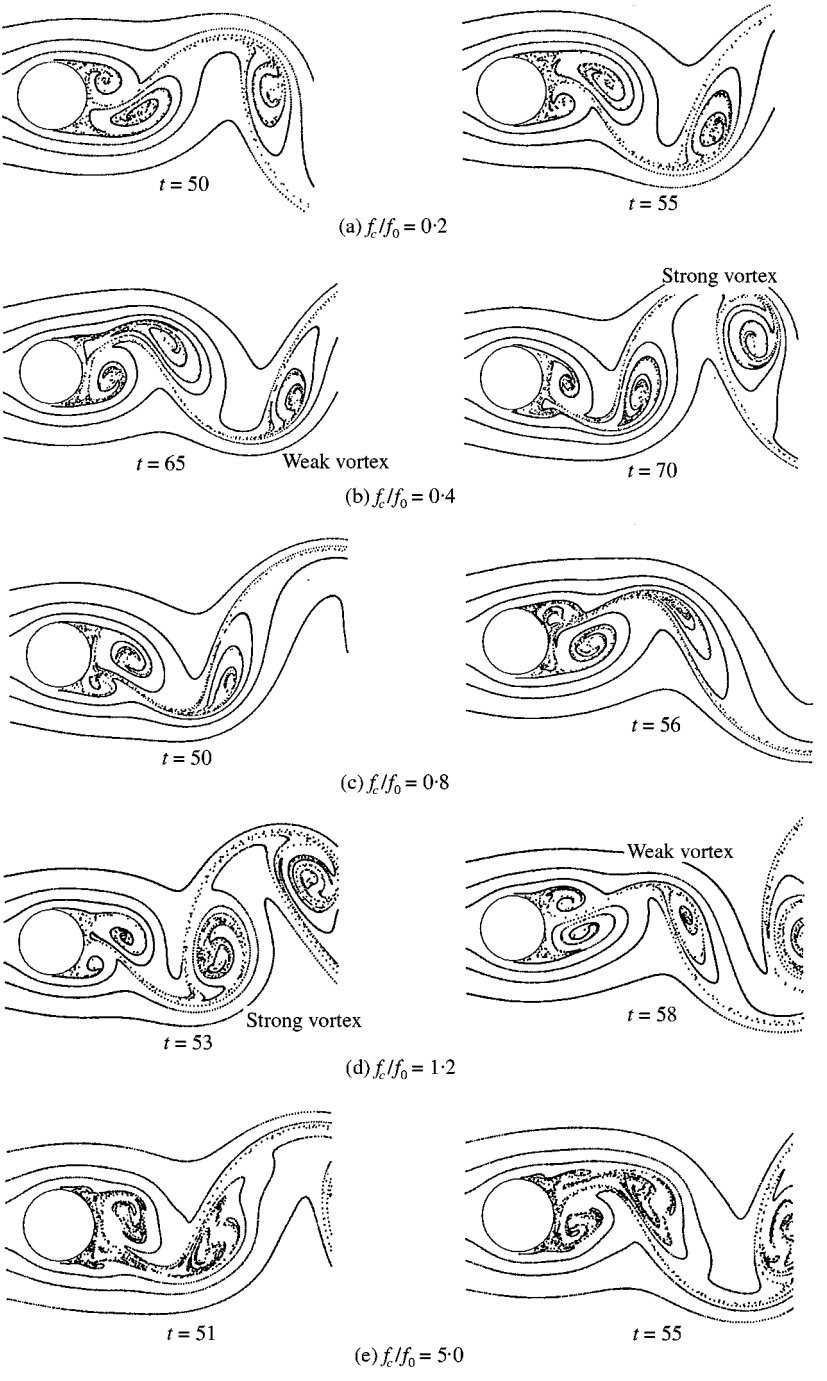

Figure 1. Patterns of instantaneous streaklines for $A_m = 0{\cdot}25$ at different frequencies f_c/f_0.

have grown to a certain level. The same phenomenon was observed by Filler *et al.* (1991) in their flow visualisation experiment at Re $= 925$. The present calculation found that the mean dimensionless time-units required for the shedding of a large-scale vortex are 6, 5·5,

and 5·2 at $f_c/f_0 = 2$, 3 and 5, respectively. When the f_c/f_0 is sufficiently high, it is found that the pattern of streakline evolution approaches the case of $f_c/f_0 = 0$. It takes about 10 dimensionless time-units for a cycle of vortex shedding to be completed. The mean value of the large-scale vortex shedding frequency estimated from 10 vortex-shedding cycles is 0·102. This is in close agreement with the value of f_v (= 0·103) for the case of $f_c/f_0 = 0$. It indicates that, when f_c/f_0 is greater than a certain limiting value, the effect of rotational oscillation is primarily confined to the flow near the cylinder, and its influence on the far-field vortex structure is insignificant. The small vortices shed in the near wake coalesce to form large-scale vortices that are similar in form and frequency to the Kármán vortex street of a stationary circular cylinder.

3.2. Surface Pressure Distribution

Figure 2 is a plot of the calculated pressure coefficient on the surface of the cylinder at different forcing frequencies for $A_m = 0{\cdot}25$. In previous experimental and numerical studies for flow past a rotationally oscillating circular cylinder reviewed in the introduction, the pressure distributions around the cylinder have not been presented. The behaviour of the pressure coefficient C_p is related to vortex shedding. For example, when a vortex is shed from the lower side of the cylinder, the fluid needs a higher velocity to pass over the upper part of the cylinder. The higher fluid velocity induces a lower surface pressure, and as a result, the pressure coefficient C_p reaches its extreme value at about the same time as when a vortex is shed. The position of minimum pressure coefficient C_p on the surface of the cylinder depends on the present positions of the vortices, which are controlled by the frequency f_c/f_0 for a fixed velocity amplitude A_m. Therefore, the minimum position C_p varies as the frequency f_c/f_0 changes.

In the case of low frequency, $f_c/f_0 = 0{\cdot}4$, Figure 2(a) shows that the position and magnitude of the minimum surface pressure vary with time. When a vortex is shed from the lower side of the cylinder at $t = 70$, the minimum suction pressure on the upper half of the cylinder reaches $-2{\cdot}4$, and its location is at $\beta \approx 90^\circ$ ($\beta = 180^\circ - \theta$). When a vortex is shed from upper side of the cylinder at $t = 75$, the minimum suction pressure location is at $\beta \approx 280^\circ$, and the value is about $-1{\cdot}5$. The asymmetry of minimum suction pressure location and its magnitude between the upper and lower half of cylinder lends further support to the uneven strength of vortex shedding and asymmetry of wake as observed previously when it is outside the lock-on range.

When $f_c/f_0 = 1$ [Figure 2(b)], the frequency f_v adjusts to the forcing frequency f_c. The variation of the pressure coefficient C_p on the surface of the cylinder with time is similar to the case of a stationary circular cylinder at the same Reynolds number (Chew *et al.* 1995), except that during lock-on the minimum pressure is shifted towards the back of the cylinder at $\beta \approx 90$ and 270°, and the value of C_p reaches about $-2{\cdot}3$, which is about 60% lower than that of the stationary cylinder. Furthermore, the fluctuation in the pressure coefficient C_p becomes larger in the range $60^\circ \leq \beta \leq 300^\circ$. Therefore, lock-on is associated with large fluctuation in the lift and drag forces due to stronger shed vortices which gain additional vorticity from the oscillating process.

As the frequency f_c/f_0 increases beyond the lock-on region, the minimum pressure shifts upstream, as shown in Figure 2(c, d). When $f_c/f_0 = 2$ [Figure 2(c)], the position of the minimum pressure coefficient C_p on the surface of the cylinder is at $\beta \approx 70$ and 290°, and the value is about -2. When $f_c/f_0 = 5$ [Figure 2(d)], the position of minimum value of the pressure coefficient C_p coincides with that of $f_c/f_0 = 0$. It indicates that the amplitudes of fluctuation in the lift and drag forces reduce when the frequency f_c/f_0 is high.

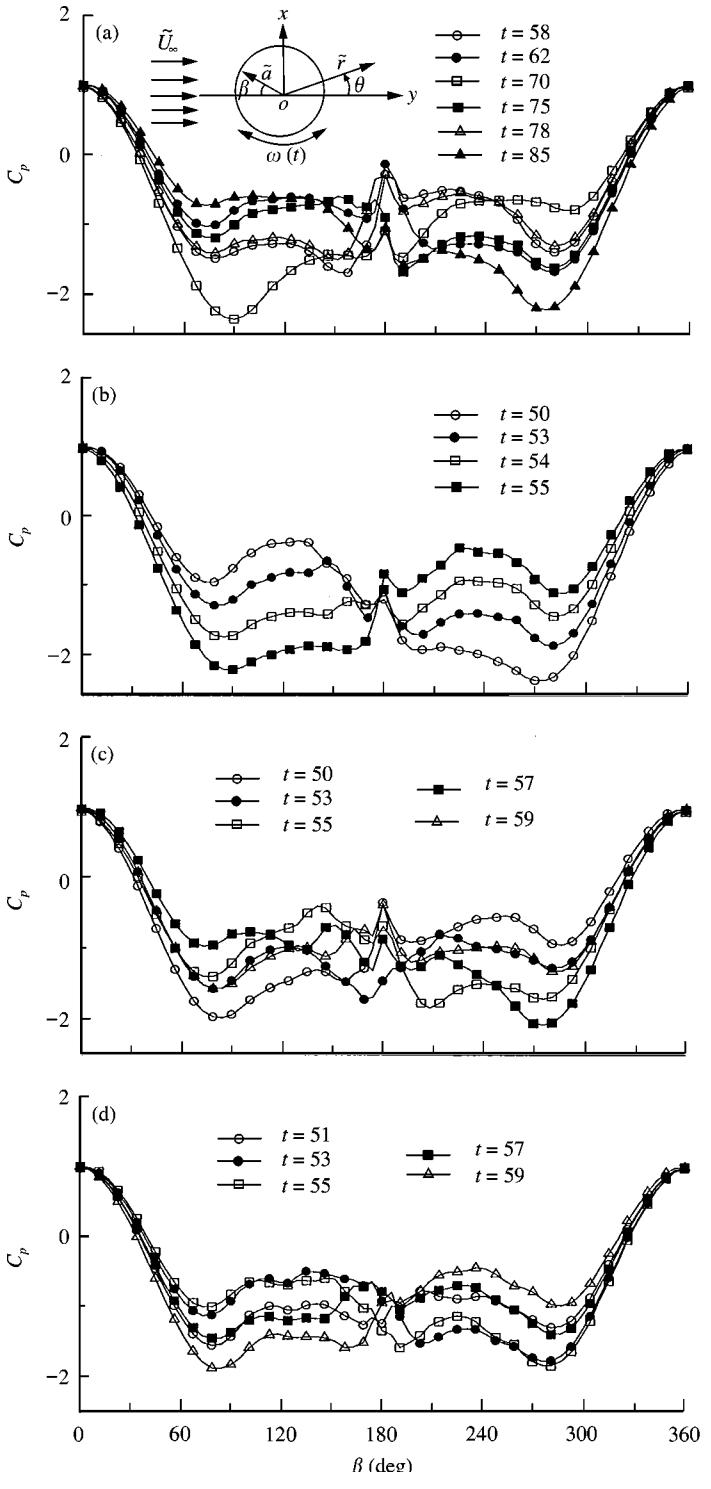

Figure 2. Pressure distribution on the surface of the cylinder for $A_m = 0{\cdot}25$ at different frequencies: (a) $f_c/f_0 = 0{\cdot}4$, (b) $f_c/f_0 = 1$, (c) $f_c/f_0 = 2$, (d) $f_c/f_0 = 5$.

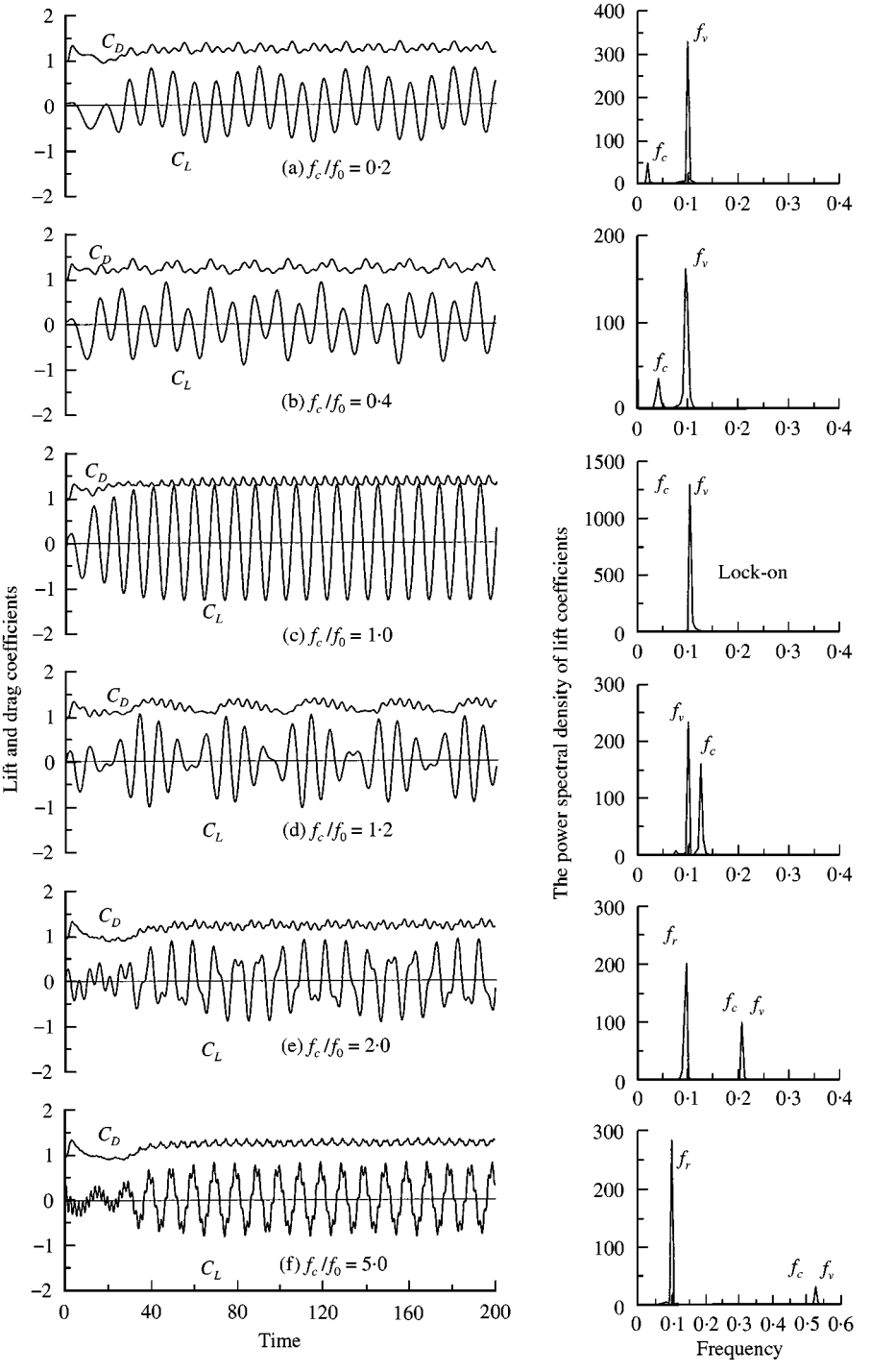

Figure 3. The time variation of C_D and C_L, and the power spectra of C_L for $A_m = 0{\cdot}25$ at different frequencies.

3.3. The Time Histories of Lift and Drag Coefficients

The time histories of the lift and drag coefficients as well as the power spectra of the lift coefficients are shown in Figure 3. When $f_c/f_0 = 0{\cdot}2$, there are two prominent frequencies in the lift spectrum as shown in Figure 3(a). They correspond to the vortex-shedding frequency f_v and forcing oscillation frequency f_c. It is clear that the frequency f_v is much more dominant. The two main-component frequencies of the lift force can clearly be observed from the lift coefficient curve. It indicates that, when f_c/f_0 is low, the interaction between f_v and f_c is very weak. The near-sinusoidal variation of the lift curve also indicates the periodic nature of vortex shedding from the cylinder. The negative peaks are caused by the shedding of vortices from the upper side of the cylinder, and *vice- versa*. As the frequency f_c/f_0 increases from 0·2 to 0·4 [Figures 3(b)], there are still two prominent frequencies in the lift spectrum, but there is a discernible drift of the vortex-shedding frequency f_v towards the forcing frequency f_c. The waveform of the lift signal, which arises from the complex interaction of the two rivalling frequencies, can be seen in Figure 3(b). The uneven amplitude of the lift force clearly supports the shedding of vortices with different strength as discussed earlier. When f_c is near f_0, f_v drifts lower and locks on to f_c, resulting in only one dominating component in the lift frequency spectrum. This is shown in Figure 3(c). During lock-on, the fluctuation amplitude of lift coefficient is larger than those outside the lock-on range, and at $f_c/f_0 = 1$, it is the highest with a peak amplitude of 1·2. This is also higher than the case of flow past a stationary cylinder which has a peak amplitude of 1 (Chew *et al.* 1995), and lends further support to our earlier proposition that "the vortices shed during lock-on are much stronger as the fluid gains additional vorticity from synchronised cylinder oscillation that provides the largest relative velocity between the cylinder wall and boundary during the vortex formation phase". When f_c/f_0 increases up to 1·2 [Figure 3(d)], the two dominant frequencies of the lift spectrum reappear, and the lift and drag coefficients become less regular. This indicates that lock-on no longer exists at $f_c/f_0 = 1{\cdot}2$, and vortices of different strength are being shed [see Figures 1(g)], resulting in amplitude variation of lift coefficient at the Kármán vortex-shedding frequency.

The behaviour of the drag coefficient variation is similar to that of lift coefficient except that it occurs at twice the latter frequency.

Table 1 summarises the behaviour of flow past a rotationally oscillating cylinder for $A_m = 0{\cdot}25$.

4. ROTATIONAL OSCILLATION WITH $A_m = 1$ AND Re = 1000

4.1. Pattern of Vortex Shedding from the Cylinder in the Near Wake

These patterns of vortex shedding at $A_m = 1$ exhibit the following behaviour: when $f_c/f_0 = 0{\cdot}2$, a pronounced feature is the shedding of a much weaker and smaller vortex once every two or three cycles, owing to the effect of the large velocity amplitude oscillation. When the frequency f_c/f_0 increases from 0·2 to 0·4, it is found that the weaker and smaller vortex mentioned above becomes increasingly weaker and smaller. It is worth noting in Figure 4(a, b) that the larger the difference in the strength of a pair of vortices shed alternatively from the cylinder, the more obvious will be their shape difference. On the other hand, comparing with small velocity amplitude oscillation of $A_m = 0{\cdot}25$ at the same frequency of $f_c/f_0 = 0{\cdot}2$, it can be observed that, as the velocity amplitude A_m of the oscillating cylinder changes, the positions of the attached vortices and the structure of vortex shedding from both sides of the cylinder also change. When $A_m = 0{\cdot}25$, the positions of the attached vortices are in the range $90^\circ \leq \beta \leq 270^\circ$, and vortices with the same size are shed alternatively from the two sides of the cylinder [see Figure 1(a)]. When $A_m = 1$,

TABLE 1
Summary of flow behaviour past a rotationally oscillating cylinder for $A_m = 0{\cdot}25$

f_c/f_0	Observed behaviour of flow
$f_c/f_0 < 0{\cdot}40$	Low cylinder-oscillation frequency is superimposed onto the Kármán vortex-shedding frequency.Vortices shed are of even strength and even spacing. Vortex street meanders at low cylinder-oscillation frequency. Amplitude of lift coefficient fluctuation at Kármán vortex-shedding frequency is uniform.
$0{\cdot}4 \leq f_c/f_0 < 0{\cdot}8$	Vortices shed are of uneven strength and irregular spacing. Vortex-shedding frequency f_v remains approximately at f_0. Amplitude of lift coefficient is irregular.
$0{\cdot}8 \leq f_c/f_0 < 1{\cdot}2$	Vortex-shedding frequency locks-on to cylinder-oscillation frequency. Vortices shed are of even strength, even spacing and strong. Amplitude of lift coefficient is large and even.
$1{\cdot}2 \leq f_c/f_0 < 2$	Same as that for $0{\cdot}4 \leq f_c/f_0 < 0{\cdot}8$.
$f_c/f_0 \geq 2$	High cylinder-oscillation frequency is superimposed onto the large-scale Kármán vortex-shedding frequency. Small-scale vortices are shed in the near wake at cylinder-oscillation frequency. Small-scale vortices coalesce in the near wake to form the large-scale Kármán vortex street of uniform vortex strength and spacing in the far wake. Amplitude of lift coefficient at Kármán vortex-shedding frequency is uniform.

vortices are still shed alternately, but vortices shed from the two sides of the cylinder can be rather different in size, and the positions of the attached vortices are in the range $70^\circ \leq \beta \leq 290^\circ$.

When $f_c/f_0 = 0{\cdot}8$ the patterns of streaklines evolution are shown in Figure 4(c). The size and strength of vortex shed increase remarkably, and $f_v = f_c$. Furthermore, one can observe a weaker secondary vortex of opposite rotation and a growing main vortex appear near the boundary layer separation points after an already formed main vortex is shed from the upper or lower side of the cylinder. This secondary vortex merges with the main vortex before shedding. When the forcing frequency increases to $f_c/f_0 = 2$, the size and strength of the vortices shed decreases further since the vortex formation time which is synchronised to f_c is shorter. Vortices are shed at the forcing frequency f_c from the upper and lower sides of the cylinder, but the regular vortex configuration in the near wake is destroyed as shown in Figure 4(d). An interesting phenomenon that can be observed in Figure 4(d) is that two oppositely signed vortices interact in the near wake and partially annihilate each other's vorticity. The remaining vorticity is then fed into the neighbouring vortices with the same sign. It implies that a new type of wake structure begins to be established in the wake slightly further away from the cylinder, and the resonance has been destroyed downstream. As f_c/f_0 increases still further, as shown in Figure 4(e), the phenomenon of vortex–vortex interaction clearly appears in the near wake, and the extent of interaction at a high f_c/f_0 is much stronger than the case at a low f_c/f_0.

Comparing Figure 4(d) with (e), one can observe that the size of vortices shed from the cylinder decreases when the rotational oscillation frequency is increased. This is expected as less time is available for each vortex to grow and be shed. At high f_c/f_0, the near-wake region is therefore occupied by a large number of small-scale vortices. Subsequently, the small-scale vortices interact with one another and merge into large-scale vortices. A growing larger-scale vortex is fed by vorticity from the small-scale vortices of the same sign, and it grows continuously until it is strong enough to draw the opposing shear layer across the wake. The approach of the oppositely signed shear layer causes the vortex to be shed and move downstream, and the process is repeated periodically and alternatively.

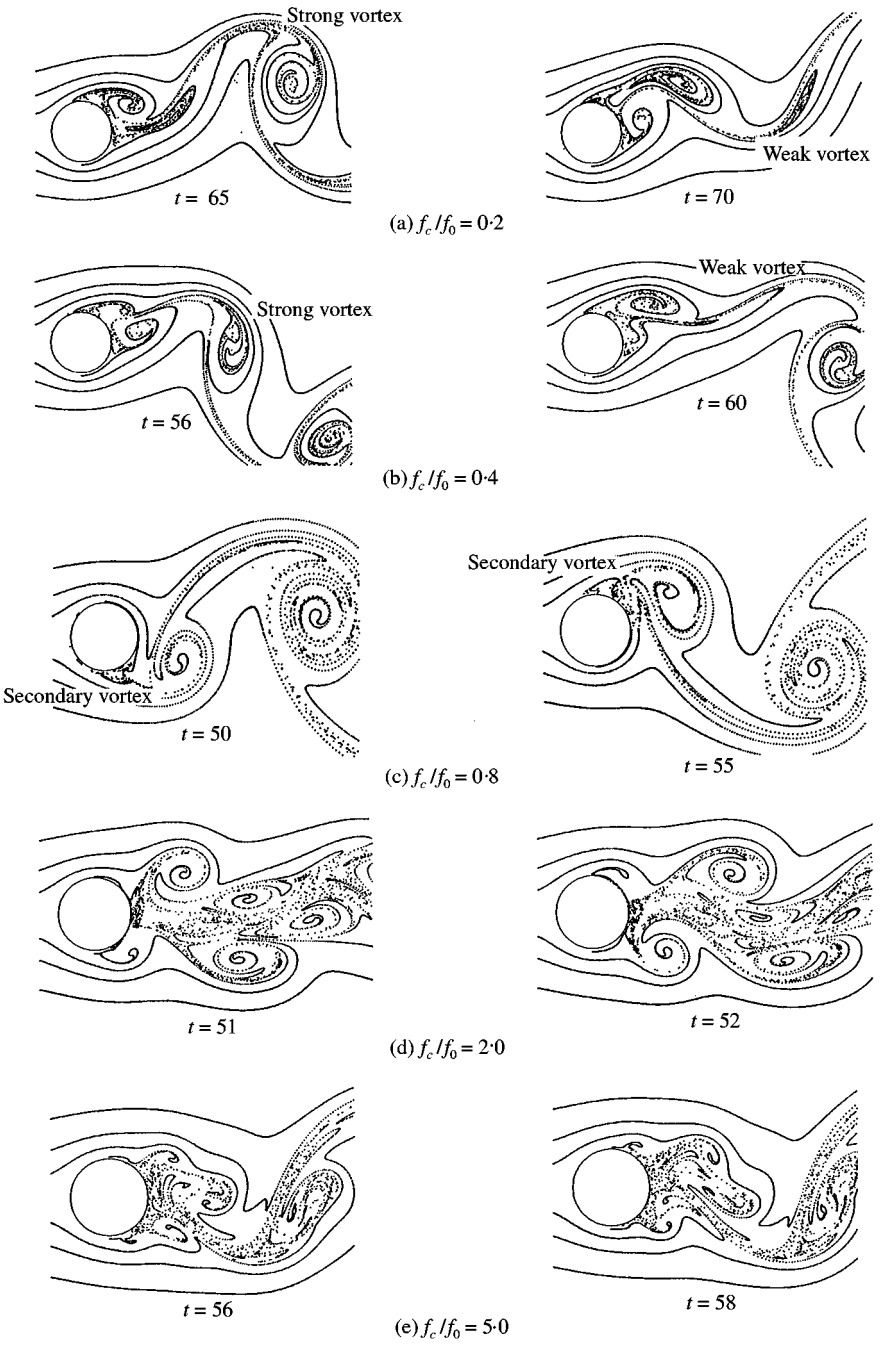

Figure 4. Patterns of instantaneous streaklines for $A_m = 1$, at different frequencies f_c/f_0.

4.2. Surface Pressure Distribution

Figure 5 shows the variation of the pressure coefficient C_p at different frequencies f_c/f_0 for the case of $A_m = 1$. This figure clearly indicates that the position of minimum surface pressure changes with the forcing frequency f_c/f_0. When $f_c/f_0 = 0{\cdot}4$ [Figure 5(a)], the

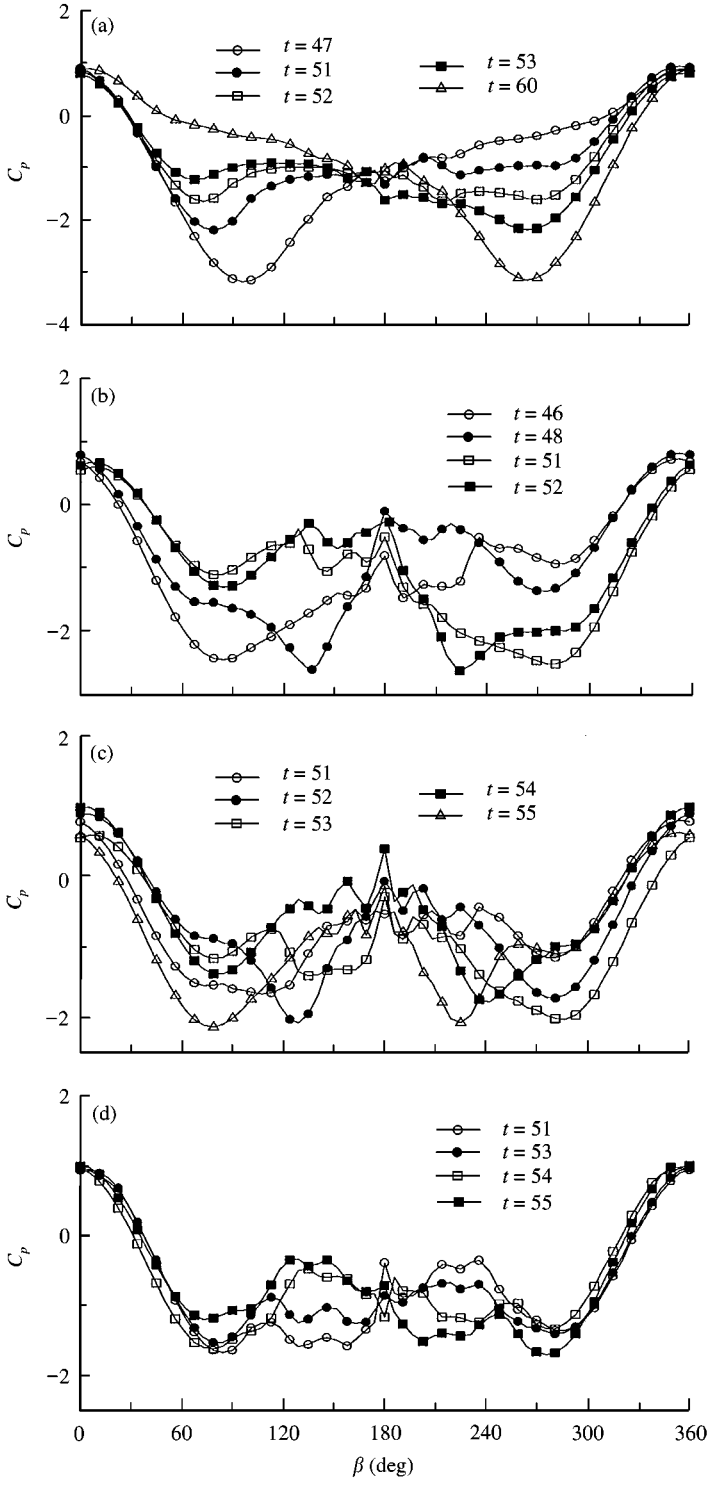

Figure 5. Pressure distribution on the surface of the cylinder for $A_m = 1$ at different frequencies: (a) $f_c/f_0 = 0{\cdot}4$, (b) $f_c/f_0 = 1$, (c) $f_c/f_0 = 2$, (d) $f_c/f_0 = 5$.

separation points change with time over a wide range so that the position of the minimum pressure varies in the range $60^\circ \leq \beta \leq 100^\circ$ and $260^\circ \leq \beta \leq 300^\circ$ on the upper and lower sides of the cylinder, respectively. When $t = 51$ and 53, corresponding to vortex shedding from the lower and upper side of the cylinder, respectively, during one cycle of vortex shedding, it is found that the minimum pressure is about -2. However, a value of $C_{p_{\min}} = -3{\cdot}2$ appears periodically and its frequency is the same as the forcing frequency f_c. The value of $C_{p_{\min}} = -3{\cdot}2$ is found at $\beta \approx 100$ and 260°.

When $f_c/f_0 = 1$ [Figure 5(b)], the frequency f_v adjusts to the forcing frequency f_c, the position of minimum surface pressure is at $\beta \approx 140$ and 220°, and the magnitude of C_p is about $-2{\cdot}6$. When $f_c/f_0 = 2$ [Figure 5(c)], the minimum C_p is about $-2{\cdot}2$, and the position varies with time. In addition, the maximum surface pressure also varies with time. When $f_c/f_0 = 5$ the position of minimum surface pressure approaches the same position($\beta \approx 80$ and 280°) as when $f_c/f_0 = 0$. However, as shown in Figure 5(d), complex pressure fluctuation appears in the region $90^\circ < \beta < 270^\circ$ as a result of the high frequency shedding of small-scale vortices.

4.3. The Time Histories of Lift and Drag Coefficients

Figure 6 shows the variation of the lift and drag coefficients with time and the power spectra of lift coefficients for $A_m = 1$. When $f_c/f_0 = 0{\cdot}2$, there are two prominent frequencies in the spectrum as shown in Figure 6(a). They correspond to the vortex-shedding frequency f_v, which is close to f_0 and the forcing oscillation frequency f_c. It is observed that the peak at f_c is higher than the peak at f_v. The lift-coefficient curve clearly resembles the shape of a sinusoidal signal at f_c that is beaten by another signal at f_v, thus indicating that there is significant interaction between the two frequencies. In the range $0{\cdot}4 \leq f_c/f_0 \leq 0{\cdot}6$, the peak at f_v diminishes in magnitude. The lift-coefficient curves show that the frequency that dominates is f_c. The power spectra also show that, unlike the case of $A_m = 0{\cdot}25$ where f_v that remains approximately at f_0 dominates, in the case of $A_m = 1$, f_c dominates and the small-scale vortex-shedding frequency f_v does not remain at $f_0 \approx 0{\cdot}1$; it drifts higher as f_c increases and is approximately 3 times the latter frequency. Although the presence of f_v is not obvious in the lift-coefficient curves, the flow is not considered to be in the lock-on range. In the present paper, lock-on is considered to have only occurred if the power spectra show one only dominating frequency.

For $0{\cdot}7 \leq f_c/f_0 < 1{\cdot}8$, the frequency of vortex shedding, f_v, locks-on to the forcing frequency f_c. It is found that the amplitude of fluctuation of both the lift and drag coefficients increases in the range $0{\cdot}7 \leq f_c/f_0 \leq 1$, and decreases in the range $1 < f_c/f_0 \leq 1{\cdot}8$. When $f_c/f_0 = 2$, two spectral peaks are seen in the lift spectrum in Figure 6(d). It thus indicates that the lock-on no longer exists. It is found that the mean value of the drag coefficient reaches its minimum, and $\bar{C}_{D_{\min}} \approx 1$. The present investigation confirms Wu's (1990) conjecture that drag could be decreased below its steady-state magnitude when the frequency is mismatched.

As f_c/f_0 further increases, the lift coefficient again exhibits the form that results from the interaction of two prominent frequencies as shown in Figure 6(e, f). The near-wake small-scale vortex-shedding frequency f_v is now locked-on to f_c and the far-wake large-scale vortex-shedding frequency f_r remains approximately at f_0 for flow past a stationary cylinder. This renders further support to the flow visualisation observation as discussed earlier. The magnitude of lift fluctuation at the frequency f_v decreases with increasing f_c as the time available for feeding of vorticity into each individual small-scale vortex decreases. The magnitude of lift fluctuation at the frequency f_r remains constant for $f_c/f_0 > 2$, indicating that the large-scale Kármán vortex street has reached some stable state.

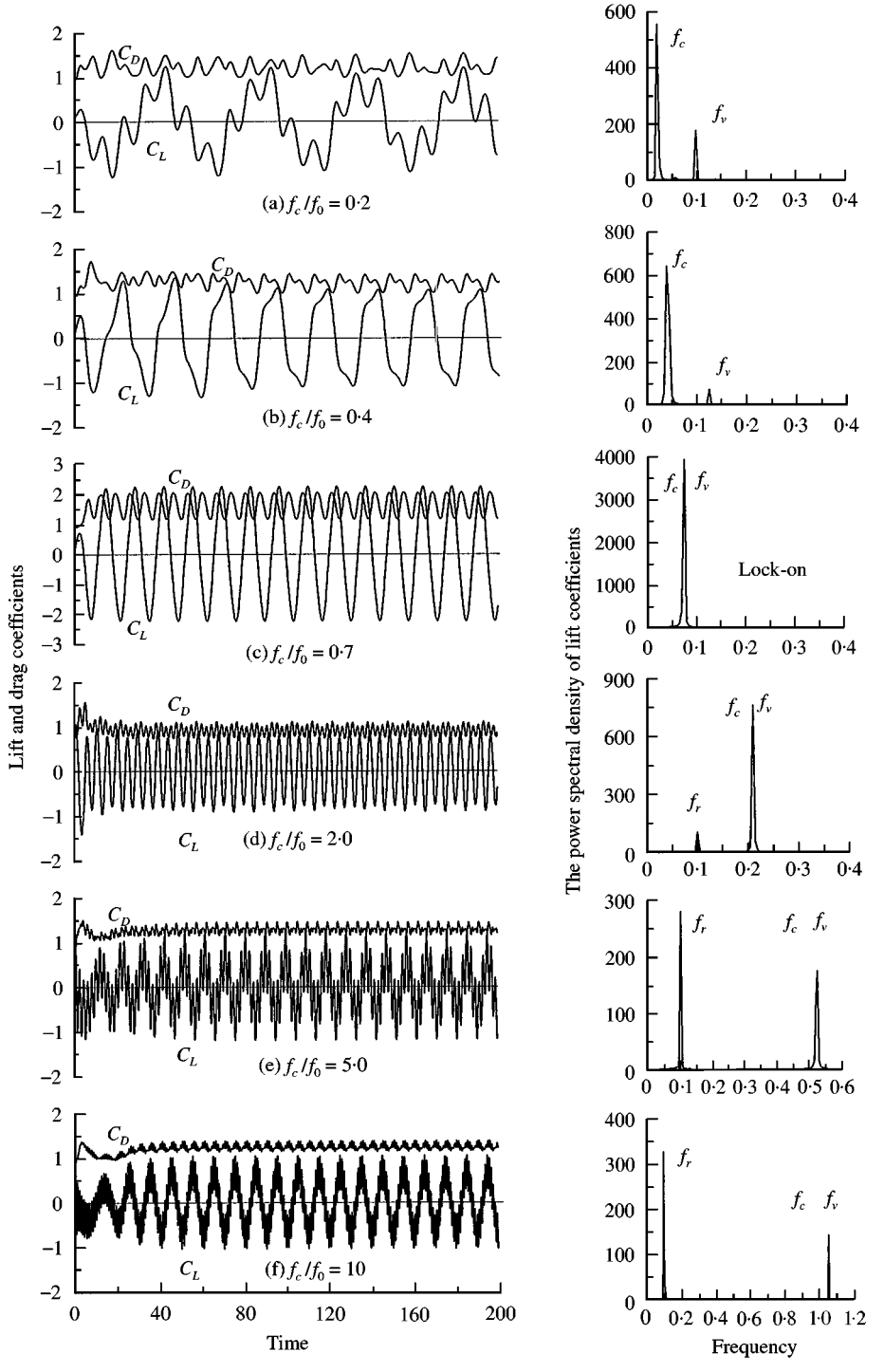

Figure 6. The time variation of C_D and C_L, and the power spectra of C_L for $A_m = 1$ at different frequencies.

TABLE 2
Summary of flow behaviour past a rotationally oscillating cylinder for $A_m = 1$

f_c/f_0	Observed behaviour of flow
$f_c/f_0 < 0{\cdot}4$	Low cylinder-oscillation frequency is superimposed onto the Kármán vortex-shedding frequency. Vortices shed are of uneven strength and spacing. Vortex street meanders at low cylinder-oscillation frequency. Amplitude of lift-coefficient fluctuation at Kármán vortex-shedding frequency is nonconstant. Coalescence of vortices occurs in the far wake.
$0{\cdot}4 \le f_c/f_0 < 0{\cdot}7$	Vortices shed are of uneven strength and irregular spacing. Vortex-shedding frequency f_v does not remain at f_0 but increases with increasing f_c. Amplitude of lift coefficient becomes more regular and constant with time as f_c increases. Coalescence of vortices occurs in the far-to-intermediate wake. As f_c increases, coalescence of vortices occurs further upstream and the resemblance of far-wake vortex street to that of stationary cylinder increases. The far-wake vortex street oscillates at f_c.
$0{\cdot}7 \le f_c/f_0 < 1{\cdot}8$	Vortex-shedding frequency locks-on to cylinder-oscillation frequency. Vortices shed are of even strength, even spacing and strong. Amplitude of lift coefficient is large, even and higher than that for $A_m = 0{\cdot}25$. It increases in the range $0{\cdot}7 \le f_c/f_0 \le 1$ and decreases in the range $1 < f_c/f_0 < 1{\cdot}8$.
$1{\cdot}8 \le f_c/f_0 < 3$	Vortices shed are slightly uneven in strength and irregular spacing. Vortex-shedding frequency f_v locks-on to f_c but fluctuation of wake at f_0 can be detected. Amplitude of lift coefficient is slightly irregular. Coalescence of vortices occurs in the near wake.
$f_c/f_0 \ge 3$	High cylinder-oscillation frequency is superimposed onto the large-scale Kármán vortex-shedding frequency. Small-scale vortices are shed in the near wake at f_c. They coalesce in the near wake to form the large-scale Kármán vortex street of uniform vortex strength and spacing in the far wake. Amplitude of lift coefficient at Kármán vortex-shedding frequency is uniform, but that at f_c decreases with increasing f_c.

Table 2 summarises the behaviour of flow past a rotationally oscillating cylinder for $A_m = 1$.

5. LARGE VELOCITY AMPLITUDE OSCILLATION WITH $A_m = 3$ AND Re = 1000

5.1. PATTERN OF VORTEX SHEDDING FROM THE CYLINDER IN THE NEAR WAKE

Owing to the large quantity of data, only some typical streakline patterns for velocity amplitude $A_m = 3$ and $f_c/f_0 \ge 0{\cdot}6$ are shown in Figure 7. When $f_c/f_0 < 0{\cdot}6$, it is found that the process of the vortex formation behind the cylinder over each half-oscillation period is similar to the case of flow past a rotating cylinder. During the first half-cycle, a vortex which is similar to the starting vortex for flow past a rotating cylinder at the rotational-to-translational speed ratio (α) of 3 [discussed in Chew *et al.* (1995)], grows slowly until it becomes almost as large as the cylinder before it is finally swept into the wake region by the free-stream flow. A mirror image situation then occurs over the second half-cycle. There are closed streamlines circulating around the cylinder. The above similarity to that observed in flow past a rotating cylinder at the speed ratio of 3 (Chew *et al.* 1995) is expected. In fact, when the forcing frequency is low but the velocity amplitude is large, during each half-cycle

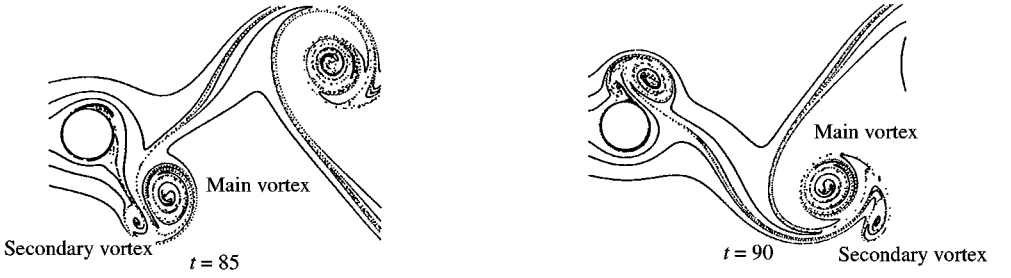

(a) $f_c/f_0 = 0{\cdot}6$

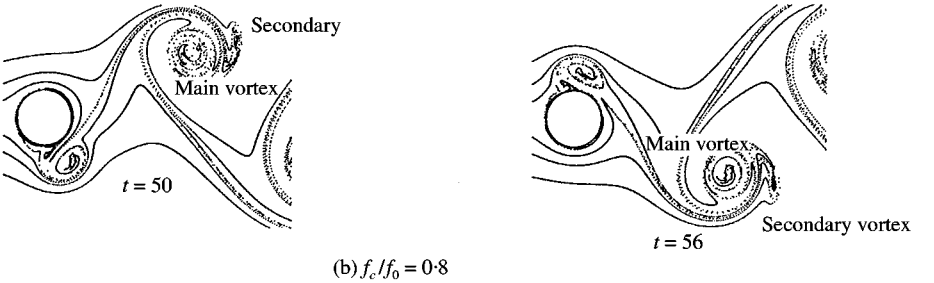

(b) $f_c/f_0 = 0{\cdot}8$

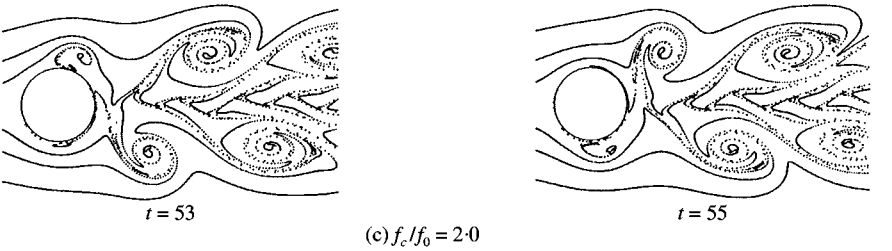

(c) $f_c/f_0 = 2{\cdot}0$

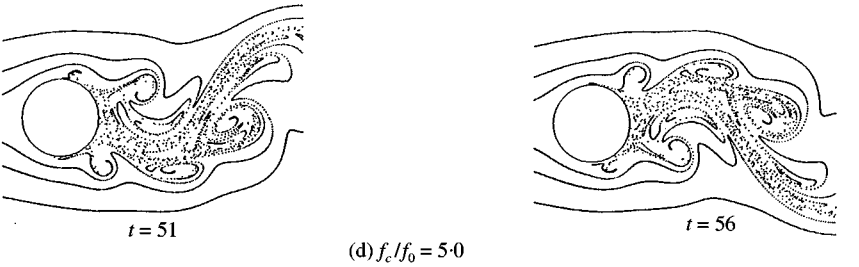

(d) $f_c/f_0 = 5{\cdot}0$

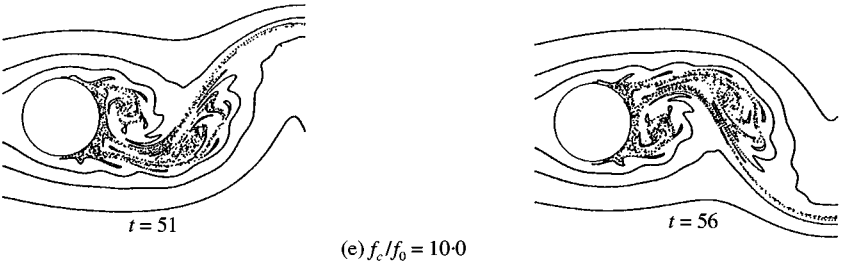

(e) $f_c/f_0 = 10{\cdot}0$

Figure 7. Patterns of instantaneous streaklines for $A_m = 3$ at different frequencies f_c/f_0.

of the oscillation, the flow "sees" the rotationally oscillating cylinder to be simply rotating with increasing speed in one direction for several revolutions before it reverses. As a result, the behaviour of flow past the above cylinder is not too different from that past a purely rotating cylinder.

When $f_c/f_0 = 0{\cdot}6$, the pattern is completely different from those cases observed at the same forcing frequency but at $A_m \leq 1$. For $A_m \leq 1$, one vortex each is shed from the upper and lower sides of the cylinder over one cycle, although occasionally the two vortices can be rather different in strength. When $A_m = 3$, however, pairs of vortices are shed in the way shown in Figure 7(a). A main vortex begins to roll up at the top of the cylinder at $t = 85$. It grows as time increases, and induces a secondary vortex of opposite sign at time $t = 90$. As time increases, a vortex pair containing two vortices of uneven strength is formed and shed from the cylinder. At this stage, another main vortex starts to roll up on the lower side of the cylinder. The paired vortex-shedding process repeats and one cycle of vortex shedding takes about 20 dimensionless time-units. This phenomenon is in agreement with the observation by Lu & Sato (1996), where computation was carried out at the same Re and forcing frequency range. It indicates that, when the forcing frequency is kept constant, greater values of A_m not only change the strength of vortices shed, but also the pattern of vortex shedding.

Figure 7(b) shows the instantaneous streakline patterns of vortex shedding at $f_c/f_0 = 0{\cdot}8$. The patterns are similar to the $f_c/f_0 = 0{\cdot}6$ case discussed above. The vortex pairs from the two shear layers appear to be regular and alternate. It is found that, as f_c/f_0 increases to 1·5, the pattern of vortex shedding remains unchanged but the longitudinal vortex spacing is reduced because of the higher f_c/f_0 involved. When the forcing frequency is increased to $f_c/f_0 = 2$ [Figure 7(c)], comparing with the case of $A_m = 1$ at the same frequency f_c/f_0, it is found that, although the regular vortex configuration in the wake is affected by vortex coalescence for $A_m = 1$ [see Figure 4(d)], there is no such change in the pattern of vortex shedding for $A_m = 3$. However, a further shortening of the vortex formation length and the longitudinal vortex spacing is observed [Figure 7(c)]. It indicates that the frequency range of lock-on increases with increasing A_m.

As f_c/f_0 increases still further, as shown in Figure 7(d), the phenomenon of vortex–vortex interaction described earlier appears in the wake. When $f_c/f_0 \geq 5$, the patterns of vortex shedding presented in Figure 7(d, e) look rather like that for $A_m = 1$ at the same frequency f_c/f_0. The small-scale vortices are shed at f_c from both sides of the cylinder, the like-sign vortices coalesce behind the cylinder and the strength of vortices shed is much stronger than that of $A_m \leq 1$. The wake structure remains essentially unchanged, even if the frequency or velocity amplitude is increased, and the streaklines in the wake exhibit similar pattern.

5.2. Surface Pressure Distribution

It is interesting to note how the coefficient C_p varies with the frequency f_c/f_0 during the oscillation motion. The present results show that the pressure distribution changes sharply at some instances. These changes are associated with the shedding of vortices, as mentioned earlier. Overall, the pressure distribution patterns have been found to be quite repeatable from one cycle to another, although they may experience some occasional changes. It is observed from Figure 8 that the positions of minimum and maximum surface pressure are forcing frequency dependent. In the case of low frequency $f_c/f_0 = 0{\cdot}4$, because the separation positions change with time over a wide range [see Figure 8(a)], the position and magnitude of the minimum surface pressure are thus also time dependent. At $t = 45$, the minimum pressure is located at $\beta = 135^\circ$ with a magnitude of about $-6{\cdot}5$. At $t = 50$, the minimum surface pressure is shifted to $\beta = 90^\circ$ and the magnitude is $C_p \approx -5{\cdot}6$. At the

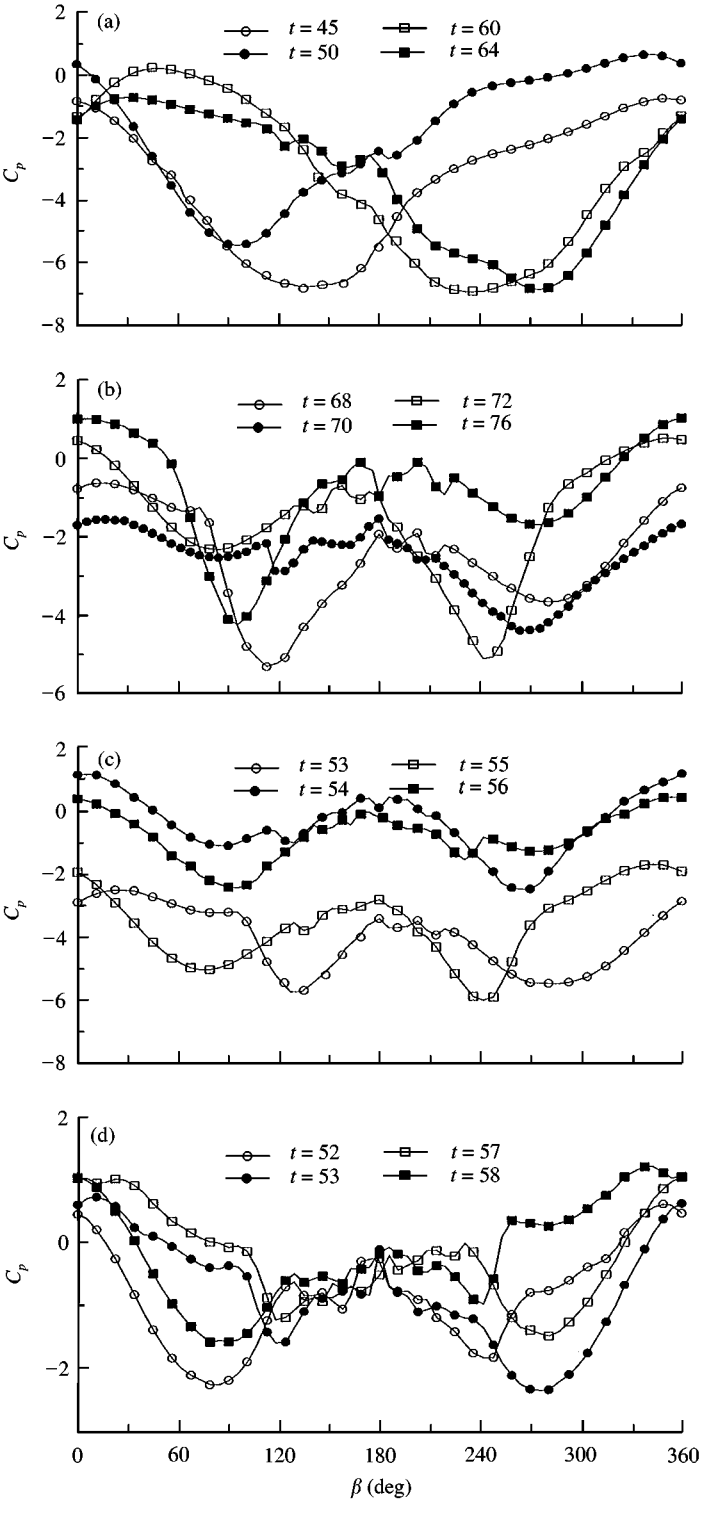

Figure 8. Pressure distribution on the surface of the cylinder for $A_m = 3$ at different frequencies: (a) $f_c/f_0 = 0{\cdot}4$, (b) $f_c/f_0 = 1$, (c) $f_c/f_0 = 2$, (d) $f_c/f_0 = 5$.

same time, the stagnation point, which is characterised by a maximum in surface pressure, also moves with time. At $t = 50$ and 60, the stagnation points are at $\beta = 340$ and 50°, respectively, and the magnitude is less than 1 because of the centrifugal force induced by rotation.

When $f_c/f_0 = 1$ [Figure 8(b)], vortices are shed alternately from the upper and lower sides of the cylinder, and the minimum surface pressure occurs at $t = 68$ and 72 and at $\beta \approx 120$ and 240°, respectively, with a magnitude of about $-5{\cdot}2$. During lock-on, the minimum surface pressure is shifted towards the back of the cylinder, resulting in large fluctuation in the drag force. Another interesting feature observed is that the pressure coefficient C_p at $\beta \approx 0°$ varies with time in range of $-1{\cdot}8 \leq C_p \leq 1$. When $f_c/f_0 = 2$, the lock-on feature can still be observed in Figure 8(c), but the difference between maximum and minimum pressure decreases. This is because the strength of vortices shed decreases on increasing the frequency f_c/f_0.

As the frequency f_c/f_0 increases out of the lock-on region [Figure 8(d)], the minimum suction pressure shifts upstream and the amplitude of the pressure variation evidently becomes smaller. Also, a complex variation in surface pressure appears in the region $90° < \beta < 270°$ because, when f_c/f_0 is high, the flow near the cylinder is dominated by the shedding of many small vortices at cylinder-oscillation frequency, as discussed previously. For $f_c/f_0 = 5$, the minimum surface pressure locations (at different t) are at $\beta \approx 75$ and 285°, and the magnitude of C_p in both cases is about $-2{\cdot}2$.

5.3. The Time Histories of Lift and Drag Coefficients

Figure 9 shows the time histories of the lift and drag coefficients as well as the power spectra of the lift coefficient for $A_m = 3$. When $f_c/f_0 = 0{\cdot}2$ [Figure 9(a)], it is clear that a low frequency component dominates the lift force. If each peak (both positive and negative peaks) in the lift-coefficient curve is related to the shedding of one vortex, then Figure 9(a) suggests that there should be eight large vortices in the wake when the dimensionless time t reaches 200 or four oscillation periods. Therefore, a vortex is shed in each half of the cycle.

The power spectral density plots of the lift coefficient in Figure 9 reveal that, when the frequency $f_c/f_0 \leq 1{\cdot}5$, besides the fundamental frequency f_c, a higher harmonic at 3 times the forcing frequency is also observed. This phenomenon can be explained with reference to vortex shedding. For large velocity amplitude A_m of oscillation, when a main vortex is formed and shed on one side of the cylinder, an adjacent secondary vortex, having opposite sign to the main vortex, is induced and is annihilated later by the main vortex. As a result, a "kink" exists at the peak and trough of the lift coefficient versus time trace and a high frequency component appears in the power spectrum. This "kink" induced by the secondary vortex after the peak (or trough) induced by the primary vortex is most obvious in Figure 9(b, c) when the secondary vortex is clearly discernible at $f_c/f_0 = 0{\cdot}6$. As the forcing frequency increases, the strength of induced secondary vortex decreases, the fluctuation generated by it becomes weaker, and eventually disappears entirely when the forcing frequency exceeds a certain value.

When the frequency $f_c/f_0 \geq 5$, as shown in Figure 9(e, f), there are also two dominating frequencies in the lift. However, unlike the cases for $f_c/f_0 \leq 1{\cdot}5$, in the present high frequency situation, one of the peaks is the forcing frequency f_c while the other is the large-scale vortex formation frequency f_r which is close to the Kármán vortex-shedding frequency for flow past a stationary cylinder.

It is difficult to define the lower boundary of the lock-on range in this case as higher harmonic frequencies are present for $f_c/f_0 \leq 1{\cdot}5$. Even at $f_c/f_0 = 0{\cdot}2$, the large-scale vortex-shedding frequency appears to be already locked-on to the cylinder-oscillation frequency f_c.

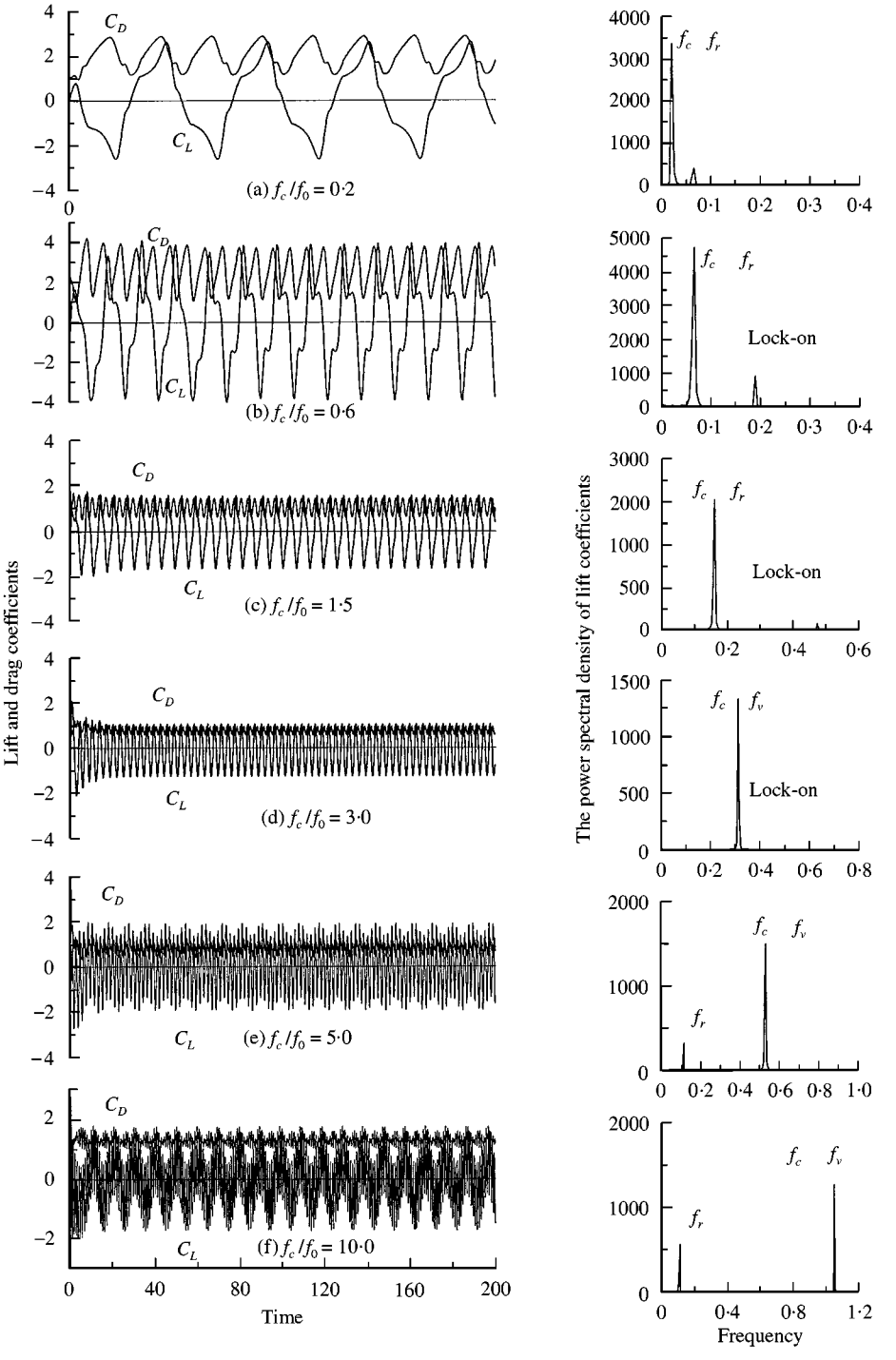

Figure 9. The time variation of C_D and C_L, and the power spectra of C_L for $A_m = 3$ at different frequencies.

TABLE 3
Summary of flow behaviour past a rotationally oscillating cylinder for $A_m = 3$

f_c/f_0	Observed behaviour of flow
$f_c/f_0 < 0{\cdot}5$	Large-scale vortex shedding at cylinder-oscillation frequency. The shed vortex is similar to the starting vortex observed for flow past a rotating cylinder at speed ratio of 3. Kármán vortex-shedding frequency is not present but the third higher harmonic of f_c is. The wake width is very wide. Amplitude of lift coefficient increases with increasing f_c.
$0{\cdot}5 \leq f_c/f_0 \leq 3$	Vortex-shedding frequency locks-on to cylinder-oscillation frequency. At $f_c/f_0 \leq 0{\cdot}8$, vortex pairs containing two vortices of uneven strength and opposite sign are shed from each side of the cylinder and the lift-coefficient curve shows kinks. Amplitude of lift coefficient is large, even higher than that for $A_m = 0{\cdot}25$ and 1. It increases with increasing f_c.
$f_c/f_0 > 3$	High cylinder-oscillation frequency is superimposed onto the large-scale Kármán vortex-shedding frequency. Small-scale vortices are shed in the near wake at f_c. They coalesce in the near wake to form the large-scale Kármán vortex street of uniform vortex strength and spacing in the far wake. The amplitude of lift coefficient at Kármán vortex-shedding frequency is uniform, but that at f_c decreases with increasing f_c.

The lower boundary was loosely defined at around $f_c/f_0 \approx 0{\cdot}5$, although a third higher harmonic frequency ($= 3\,f_c$) is still present. It was chosen mainly because the wake width has begun to narrow down. The upper boundary of the lock-on range was defined when the small-scale vortices in the near wake coalesce to form a large-scale vortex street which begins to appear at the Kármán vortex-shedding frequency f_0.

Table 3 summarises the behaviour of flow past a rotationally oscillating cylinder for $A_m = 3$.

6. THE GLOBAL CHARACTERISTICS OF FLOW

Figure 10 shows the variation of the root-mean-square value of the lift coefficients with the forcing frequency and velocity amplitude. It is observed that all the fluctuations in the lift coefficients peak in the vicinity of $f_c \approx f_0$ (i.e., $f_c/f_0 \approx 1$) and its higher harmonics. As expected, the peak value is the largest near f_0, and diminishes in amplitude with increasing harmonics of f_0. The r.m.s. values of the drag coefficients behave similarly. The present results are in agreement with the experimental results of Okajima *et al.* (1975).

Figure 11 describes the variation of the mean values of the drag coefficients $\bar{C}_D$ with the oscillation frequency and velocity amplitude. The maximum mean drag over the range shown increases with increasing velocity amplitude. When $A_m = 0{\cdot}25$, 0·5, 1, 2 and 3, the maximum $\bar{C}_D$ is 1·4, 1·6, 1·8, 2·4 and 2·9 and occurs at $f_c/f_0 \approx 1$, 0·9, 0·85, 0·7 and 0·6, respectively. This is within the lock-on range of the respective A_m. When lock-on occurs, the vortices formed in the near-wake region are strong resulting in higher suction pressure. This is supported by the pressure distribution curves presented in Figures 2, 5 and 8. The locked-on vortices increase in strength with increasing A_m as stronger vorticity generated by the moving wall is being fed to the vortices, and thus the maximum $\bar{C}_D$ is higher at large A_m.

The shift in the peak of $\bar{C}_D$ to lower f_c/f_0, i.e., lower end of lock-on range, as A_m increases may be explained by the vortex formation time. As f_c/f_0 decreases, the vortex formation time within the lock-on range at fixed A_m increases, resulting in more vorticity being fed to the near-wake vortices. This leads to $\bar{C}_D$ peaks at the lower f_c/f_0 end of the lock-on range at

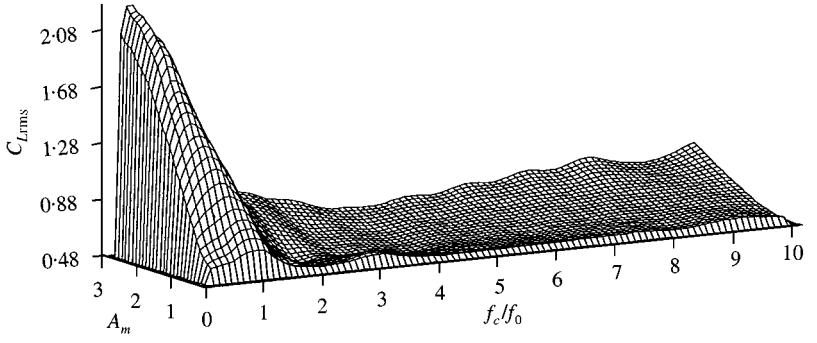

Figure 10. Variation of r.m.s. value of lift coefficients with A_m and f_c/f_0.

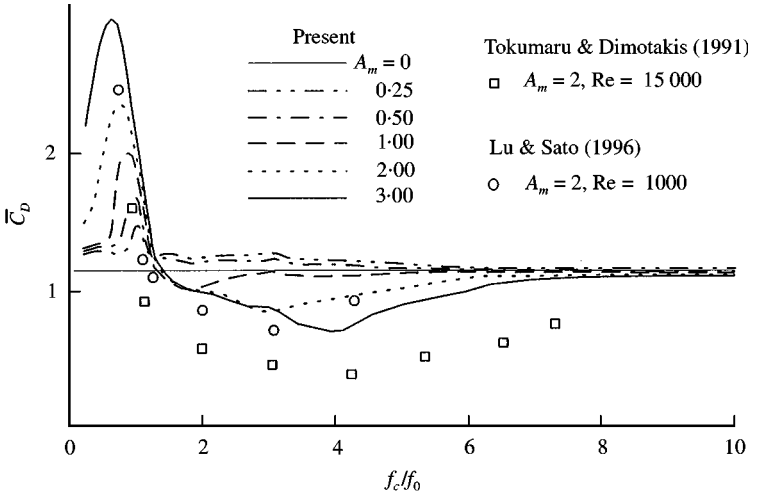

Figure 11. Variation of mean value of drag coefficients with A_m and f_c/f_0.

a particular A_m. As the lock-on range increases with increasing A_m, the peak of $\bar{C}_D$ thus shifts to lower f_c/f_0 at higher A_m.

It is interesting to note that, when $A_m = 1$, 2 and 3, the mean value of the drag coefficient reaches a minimum of 1, 0·9 and 0·7 at $f_c/f_0 \approx 1{\cdot}8$, 3 and 4, respectively, which is lower than the mean value of the drag coefficient of a stationary cylinder. This tendency becomes more evident as the velocity amplitude increases. The reason is that the frequencies are mismatched when lock-on ends and a new vortex configuration is formed in the wake. The mismatch of cylinder oscillation and vortex-shedding frequencies may have prevented the formation of strong vortices in the near wake resulting in a lower near-wake suction pressure. When $A_m = 2$, the present result is in close agreement with the result of Lu & Sato (1996) at the same Reynolds number. Furthermore, the present results follow the trend reported by Tokumaru & Dimotakis (1991) at $\mathrm{Re} = 1{\cdot}5 \times 10^4$. The discrepancies with their results could be due to the Reynolds number or three-dimensional effects. The rotational oscillation at very large magnitudes can produce significant reduction in the drag acting on the cylinder when the forcing frequency and the stationary cylinder vortex-shedding

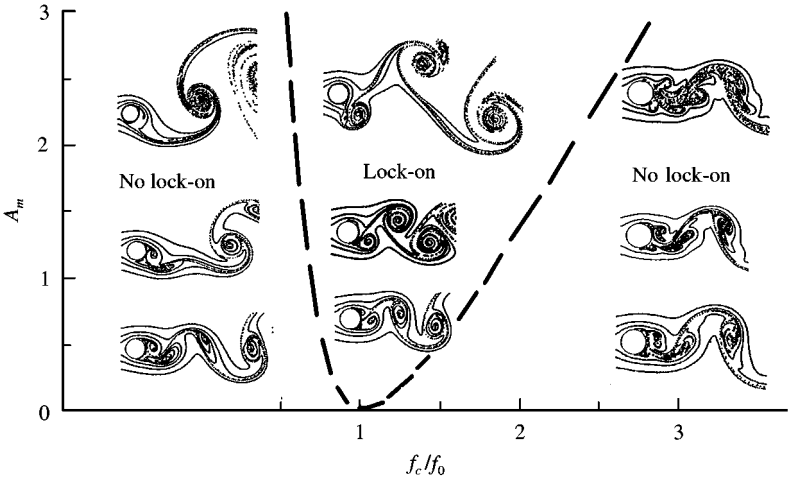

Figure 12. The fundamental lock-on band and vortex structure in the near wake.

frequency are mismatched. For example, at $A_m = 3$ and $f_c/f_0 = 4$, a 40% reduction in the mean drag can be achieved.

One of the objectives of investigating flow past an oscillating body is to determine the lock-on range. In the present result, the boundary between the lock-on and no lock-on regimes is estimated from the spectral analysis of lift coefficients and vortex structure in the near wake. The lower limit of lock-on is located at $f_v = f_c$ and $f_c < f_0$. The upper limit of lock-on is located where f_r, the frequency associated with the reappearance of Kármán vortices due to coalescence of small-scale vortices, begins to appear.

The classification of the different vortex structures in the near wake and the relationship between the range of lock-on frequencies and A_m for the present investigation is shown in Figure 12. When $A_m = 0{\cdot}25$, lock-on occurs in the range $0{\cdot}8 \leq f_c/f_0 < 1{\cdot}2$. When $A_m = 1$, it is in the range $0{\cdot}7 \leq f_c/f_0 < 1{\cdot}8$. When $A_m = 3$, the range becomes $0{\cdot}5 \leq f_c/f_0 \leq 3$.

7. CONCLUSIONS

Based on the numerical investigation conducted at various A_m and f_c/f_0, the following conclusions can be made.

1. For $A_m < 1$, when the frequency f_c/f_0 is very low, vortices are shed at frequency $f_v\,(\approx f_0)$ from the cylinder. Vortices shed are of even strength and spacing. The vortex street meanders at a low cylinder-oscillation frequency. When the frequency f_c/f_0 is below the lock-on frequency, the vortices shed are of uneven strength and irregular spacing. The vortex-shedding frequency f_v remains approximately at f_0 and the amplitude of the lift coefficient is irregular.

2. For $A_m = 1$, when the frequency f_c/f_0 is below the lock-on frequency, although the vortices shed are of uneven strength and irregular spacing, the vortex-shedding frequency f_v does not remain at f_0 but increases with increasing f_c. The amplitude of the lift coefficient becomes more regular and constant with time as f_c increases. The coalescence of vortices occurs in the intermediate-to-far wake. As f_c increases, coalescence of vortices occurs further upstream and the resemblance of the far-wake vortex street to that of a stationary cylinder increases. The far-wake vortex street oscillates at f_c.

3. For $A_m > 1$, when the frequency f_c/f_0 is very low, large-scale vortices are shed at cylinder-oscillation frequency. The wake is very wide. When the frequency f_c/f_0 is below the lock-on frequency, vortex pairs of uneven strength are shed from each side of the cylinder and the lift-coefficient curve shows kinks.

4. For all A_m, when the frequency f_c/f_0 is close to 1, the vortex shedding is locked-on to the forcing frequency in the classical manner, and the form of vortex shedding and lock-on exhibit a particularly strong resonance between the flow perturbations and the vortex wake. The lock-on frequency range increases with increasing velocity amplitude A_m, and at $A_m = 0{\cdot}25$, 1 and 3, the f_c/f_0 ranges are 0·8–1·2, 0·7–1·8 and 0·5–3, respectively.

5. For all A_m, when the frequency f_c/f_0 is greater than 1 in the post-lock-on range, the vortices are shed at frequency $f_v = f_c$ in the near wake. The size of vortices shed decreases with increasing f_c/f_0, and the strength of vortices shed increases with increasing A_m. The range of frequency ratio f_c/f_0 over which cylinder oscillation dictates the vortex-shedding frequency f_v increases as the oscillation velocity amplitude A_m increases. Over a wide range of f_c/f_0, the vortices shed at the frequency f_c from the cylinder interact in the wake and result in a large-scale antisymmetrical structure with the frequency f_r. This large-scale vortex structure is similar in form and frequency to the Kármán vortex street downstream of a stationary cylinder. The frequency f_r varies with increasing f_c/f_0 and is approximately equal to the frequency f_0 when $f_c/f_0 > 5$.

6. The root-mean-square values of the lift and drag coefficients increase remarkably when the cylinder oscillates with a frequency that is at or near f_0. Lock-on is associated with large fluctuations in the lift and drag forces. When $A_m = 0{\cdot}25$, 0·5, 1, 2 and 3, the maximum $\bar{C}_D$ is 1·4, 1·6, 1·8, 2·4 and 2·9 and occurs at $f_c/f_0 \approx 1$, 0·9, 0·85, 0·7 and 0·6, respectively, within the lock-on range, i.e., the peak increases with increasing A_m and shifts to the lower frequency end of the lock-on range. When the frequency ratio is greater than a certain value beyond the lock-on range, the mean value of the drag coefficients $\bar{C}_D$ decreases with increasing f_c/f_0. The larger the amplitude of oscillation, the more distinct is the decrease in drag coefficient. When $A_m = 1$, 2 and 3, the minimum $\bar{C}_D$ is 1, 0·9 and 0·7 and occurs at $f_c/f_0 \approx 1{\cdot}8$, 3 and 4, i.e., lower than that for flow past a stationary cylinder. After the minimum is reached, the drag coefficient increases again with increasing f_c/f_0 and approaches the value of the stationary cylinder.

ACKNOWLEDGEMENTS

This paper arises in part from the Ph.D. research of the first author. The authors are grateful to the late Dr David Maull of Cambridge University, the examiner of the Ph.D. thesis, for his helpful comments and discussion, more of which will be sadly missed.

REFERENCES

BAEK, S. J. & SUNG, H. J. 2000 Quasi-periodicity in the wake of a rotationally oscillating cylinder. *Journal of Fluid Mechanics* **408,** 275–300.

BEARMAN, P. W. 1984 Vortex shedding from oscillating bluff bodies. *Annual Review of Fluid Mechanics* **16,** 195–222.

BEARMAN, P. W. & CURRIE, I. G. 1979 Pressure fluctuation measurements on an oscillating circular cylinder. *Journal of Fluid Mechanics* **91,** 661–677.

BISHOP, R. E. D. & HASSAN, A. Y. 1964 The lift and drag forces on a circular cylinder oscillating in a flowing fluid. *Proceedings of the Royal Society* (*London*) **A 277,** 51–75.

CHENG, M., CHEW, Y. T. & LUO, S. C. 1997 A hybrid vortex method for flows over bluff body. *International Journal for Numerical Methods in Fluids* **24,** 253–274.

CHEW, Y. T., CHENG, M. & LUO, S. C. 1995 A numerical study of vortex shedding from a rotating circular cylinder by a hybrid vortex method. *Journal of Fluid Mechanics* **299,** 35–71.

CHOU, M. H. 1997 Synchronization of vortex shedding from a cylinder under rotary oscillation. *Computers and Fluids* **26,** 755–774.

DENNIS, S. C. R., NGUYEN, P. & KOCABIYIK, S. 2000 The flow induced by a rotationally oscillating and translating circular cylinder. *Journal of Fluid Mechanics* **407,** 123–144.

FILLER, J. R., MARSTON, P. L. & MIH, W. C. 1991 Response of the shear layers separating from a circular cylinder to small-amplitude rotational oscillations. *Journal of Fluid Mechanics* **231,** 481–499.

GRIFFIN, O. M. & HALL, M. S. 1991 Review of vortex shedding lock-on and flow control in bluff body wakes. *ASME Journal of Fluids Engineering* **113,** 526–537.

GRIFFIN, O. M. & RAMBERG, S. E. 1974 The vortex-street wakes of vibrating cylinders. *Journal of Fluid Mechanics* **66,** 553–576.

KOOPMANN, G. H. 1967 The vortex wakes of vibrating cylinders at low Reynolds numbers. *Journal of Fluid Mechanics* **28,** 501–512.

LU, X. Y. & SATO, J. 1996 A numerical study of flow past a rotationally oscillating circular cylinder. *Journal of Fluids and Structures* **10,** 829–849.

MENEGHINI, J. R. & BEARMAN, P. W. 1995 Numerical simulation of high amplitude oscillatory flow about a circular cylinder. *Journal of Fluids and Structures* **9,** 435–455.

OKAJIMA, A., TAKATA, H. & ASANUMA, T. 1975 Viscous flow around a rotationally oscillating circular cylinder. Reports of Institute of Space and Aeronautical Science (University of Tokyo), No. 532, pp. 311–338.

ONGOREN, A. & ROCKWELL, D. 1988*a* Flow structure from an oscillating cylinder. Part 1. Mechanisms of phase shift and recovery in the near wake. *Journal of Fluid Mechanics* **191,** 197–223.

ONGOREN, A. & ROCKWELL, D. 1988*b* Flow structure from an oscillating cylinder. Part 2. Mode competition in the near wake. *Journal of Fluid Mechanics* **191,** 225–245.

TANEDA, S. 1972 Visualization experiments on unsteady viscous flows around cylinders and plates. In *Récentes Recherches sur les Couches Limites Instationnaires* (ed. E. A. Eichel Brenner) Vol. **2,** pp. 1165. Quebec, Canada: Laval University Press.

TANEDA, S. 1978 Visual observations of the flow past a circular cylinder performing a rotatory oscillation. *Journal of the Physical Society of Japan* **45,** 1038–1043.

TOKUMARU, P. T. & DIMOTAKIS, P. E. 1991 Rotary oscillation control a cylinder wake. *Journal of Fluid Mechanics* **224,** 77–90.

WILLIAMSON, C. H. K. & ROSHKO, A. 1988 Vortex formation in the wake of an oscillating cylinder. *Journal of Fluids and Structures* **2,** 355–381.

WU, J. M. 1990 On oscillating shear layer excitation of a cylinder. *Engineering Science, Fluid Dynamics* pp. 341–351. Singapore: World Scientific Publishing Company.

WU, J. M., MO, J. D. & VAKILI, A. D. 1989 On the wake of a cylinder with rotational oscillations. *AIAA* paper 89–1024.